



# An efficient electrochemical optimizer for the distribution of relaxation times of lithium-ion batteries

Pengcheng Niu <sup>a,b</sup>, Kun Yang <sup>a,\*</sup>, Zhengxiang Song <sup>a,b</sup>, Zheyuan Pang <sup>a,b</sup>, Zhuoyu Feng <sup>a</sup>, Jinhao Meng <sup>a</sup>

<sup>a</sup> School of Electrical Engineering, Xi'an Jiaotong University, Xi'an, 710049, China

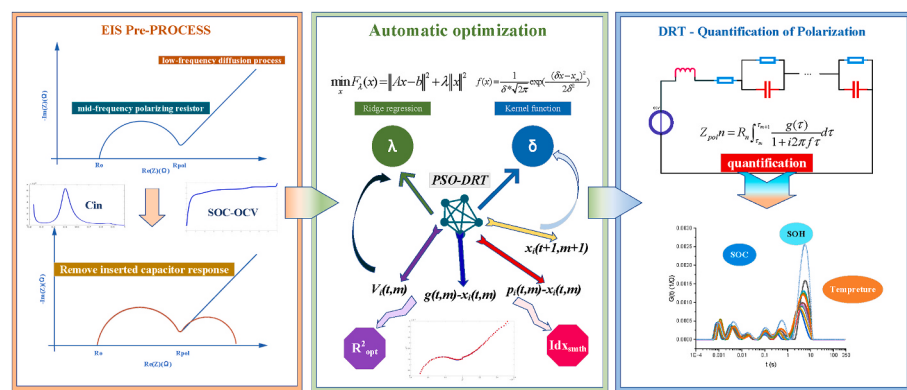
<sup>b</sup> State Key Laboratory of Electrical Insulation and Power Equipment, Xi'an, 710049, China



## HIGHLIGHTS

- The accurate implementation of full-frequency DRT considering the inserted capacitor.
- Optimize the regularization parameter and FWHM to avoid overfitting and underfitting.
- Multiple objective constrained optimization automatically obtains perfect DRT results
- A new DRT pre-processing tool for different frequency points and SOCs are available

## GRAPHICAL ABSTRACT



## ARTICLE INFO

### Keywords:

Distribution of relaxation times  
Electrochemical impedance spectroscopy  
Parameter optimization  
Preprocessing

## ABSTRACT

The distribution of relaxation times (DRT) analysis based on Tikhonov regularization is widely used to analyze the battery electrochemical impedance spectroscopy (EIS), but the selection of the regularization parameter has always been a problem. This paper proposes an Optimization Pre-calculation DRT-tool of EIS (OPDEIS) which not only completes the full-frequency EIS fitting with the insertion capacitor and inductance but also obtains the optimal regularization parameter and the fitting kernel function width through a multi-objective optimization algorithm. In particular, it can resolve the DRT parameter selection for EIS above 0.1 Hz in lithium-ion batteries effectively. This optimizer is suitable for lithium-ion battery EIS data with different states of charge (SOCs) and frequency points. It provides a reference for selecting the regularization parameter and full width at half maximum (FWHM) automatically, enabling the DRT process based on Tikhonov regularization to perfectly avoid overfitting or underfitting.

\* Corresponding author.

E-mail address: [kun.yang@xjtu.edu.cn](mailto:kun.yang@xjtu.edu.cn) (K. Yang).

## Nomenclature

$R_o$	Ohmic internal resistance
$R_{pol}$	Polarization resistance
$f$	Frequency
$\tau$	Relaxation time
$\omega$	angular velocity
$w_n$	Weighting function for the complex nonlinear least squares fitting
$C_{in}$	Inserting capacitance
$Q_{li}$	Actual capacity of a battery
$p$	Parameters of polynomial fitting
$L$	Second derivative differentiation matrix
$g(\tau)$	Distribution function of relaxation times
$X_n$	Weight applied to each basis function
$\Phi(t)$	Discretization basis
$e_g(t)$	$Z_{exp} - Z_{fit}$ Fitting error of each basis function Actual impedance Fit impedance with DRT model
$\lambda$	Regularization parameter
$\mu$	Width parameter of basis function
$K$	Curvature
$S_{ch}$	Number of extremal points
$R_{opt}^2$	Accuracy index
$Idx_{smth}$	Smoothness index

## 1. Introduction

The EIS of the batteries is now considered as an effective tool for monitoring battery information [1]. Recent studies indicate a close correlation between internal failures [2] and capacity degradation [3] in lithium-ion batteries and changes in impedance. The EIS curve contains a vast amount of internal information about the battery, which is currently used to estimate the state of charge (SOC) [4,5], state of health (SOH) [6,7], internal temperature of the battery [8], and so on. The deconstruction of information from an EIS curve typically involves three methods. The first method is parameter identification based on equivalent circuit models (ECMs) [9,10]. In addition to ECMs, data-driven deconstruction through the use of neural network methods to correlate the impedance spectra is widely used [11,12]. Lastly, researchers often extract and analyze the battery characteristics using a combination of electrochemical modeling and data-driven methods [13–15]. In the above methods, only the frequency information provided by EIS is utilized to obtain desired application results, without analyzing the internal kinetics of the battery.

The DRT is a reliable analysis approach of EIS that converts information from the frequency domain to the time domain. The battery's internal electrochemical reactions correspond to changes in the time domain [16]. The DRT method is widely employed in analyzing impedance spectra of lithium-ion batteries, Polymer Electrolyte Membrane (PEMs), and Solid Oxide Fuel Cells (SOFCs) [17,18]. In the timescale, DRT can not only provide obvious differences in voltage, current, and SOCs compared to conventional EIS but it also can be used to accurately evaluate the internal dynamic processes of the battery. Additionally, it is capable of effectively distinguishing the polarization resistances of various stages of the anodic and cathodic reaction processes within the battery, offering an alternative analytical approach for studying the electrolyte and diffusion phenomena inside the battery [19, 20]. The DRT method deconstructs the EIS curve with decoupled semicircles on a time-constant scale [21]. Consequently, the battery transitions from an inherent gray box or black box model to a clear battery dynamic structure. For lithium-ion batteries, DRT can provide early warning and monitoring of internal battery faults, helping to prevent potential dangers during operation. Meanwhile, DRT can also

estimate the battery's lifespan, guide the battery's cycling utilizations, evaluate the battery's consistency [22,23], and further optimize the battery electrode manufacturing process, etc.

The DRT method is a  $n$ th-order extension of equivalent circuit models with RC circuits. It is typically calculated using Tikhonov regularization [24,25], impedance spectrum genetic programming algorithms (ISGP) [26], Gaussian processes [27,28], maximum entropy method [29], and Fourier analysis [30]. The regression models of the maximum entropy method and the ISGP have relatively higher complexity and relatively longer convergence time. Gaussian process regression and Tikhonov regularization are similar regression models when the basic functions are radial basis functions (RBFs), and both require the selection of hyperparameters. Tikhonov regularization is widely used due to its fast convergence speed and adjustability in fitting. However, there are still some usage issues with the DRT based on Tikhonov regularization.

Tikhonov regularization can exhibit non-convergence due to the low-frequency pure capacitive behavior in EIS. The low-frequency part of the lithium-ion battery EIS exhibits diffusion phenomena similar to pure capacitive effects lacks convergent characteristics, and cannot be fitted with a typical RC parallel model. In the study of low-frequency [31], used the capacitance to simulate low-frequency tail divergence characteristics, but its model only extracted the insertion capacitance for a few specific SOCs. Iurilli used Warburg impedance to simulate low-frequency EIS [32,33]. However, this approach overlooked the diffusive process of coupling in the low-frequency range.

The regularization parameter in Tikhonov regularization has a large impact on the results. A large regularization parameter can lead to each peak being flat, causing the characteristic peaks of DRT to be coupled together and difficult to separate. In contrast, a small regularization parameter can result in unnecessary false peaks and burrs. These phenomena are unfavorable for further integration calculations. Osinkin, D. A.'s study used the least squares method combined with the DRT function to determine the selection of regularization parameters [18]. Ciucci's study checked the real and imaginary parts to select the optimal regularization parameter [34,35]. Hansen's study used the L-curve to address the parameter optimization problem [36,37]. These methods were often used to obtain the size of the regularization parameter. In addition to the regularization parameter, the selection of the full width at half maximum (FWHM) also affects results which is often overlooked by researchers. It means the influence of each function on the timescale. A large FWHM can cause excessive interference from multiple functions at a certain point, resulting in coupled peaks without characteristics. A small FWHM can cause each peak to only affect a short period, ultimately leading to oscillations in the results.

There are also some other studies regarding Tikhonov regularization. Li et al. combined Lasso and Ridge regularization using elastic net to fit EIS, but they did not optimize the specific parameters of Ridge regression [38]. Schlüter, N. .et al. used variance tests based on multiple measurements of impedance to obtain the optimal regularization parameter, but this method was time-consuming and cannot intelligently select parameters for different frequency ranges [39,40]. Hahn, M. et al. focused on the impact of the selection of the number of time constants in the distribution of DRT processes [41]. Zhang, Y. et al. proposed a method that did not require pre-determination of the regularization parameter [42]. It considered the regularization parameter as a distribution in the time domain, thereby obtaining a well-fitted DRT solution. However, this method is not suitable for further studies on changes in lithium-ion batteries and lacks strong interpretability at certain time constants [43]. Zhu, D. et al. investigated the influence of the number of RBFs on DRT and proposed characteristic frequencies based on this [44], but it limited the impact of the basis functions on the results from another perspective. However, they did not study the optimization impact of regularization parameters and the width of the basis functions.

The optimization pre-calculation DRT tool for EIS (OPDEIS)

proposed in this paper is a new method for DRT specifically designed for automatic optimization of EIS. The main work and contributions of the study are as follows:

- (1) OPDEIS obtains accurate insertion capacitance through 1/100C discharge experiments. The capacitance is then used to fit diffusion in the low-frequency range and extend the DRT to the entire frequency range. It addresses the non-convergence issue in the DRT method for analyzing the EIS of lithium batteries. Simultaneously, it preserves low-frequency information.
- (2) OPDEIS utilizes the MOPSO algorithm, combined with the proposed accuracy and smoothness objectives, to accomplish the selection of regularization parameter and FWHM parameter in the full frequency range of the DRT. OPDEIS will automatically optimize based on EIS data with different impedance magnitudes and different points per decade (ppd) of EIS data. Compared to existing research, this method accelerates the convergence speed of optimization for selecting regularization parameters. Additionally, it considers the influence of basis function width. By employing the error-index and smoothness index as dual objectives, the obtained DRT results show no occurrence of pseudo peaks or overfitting phenomena. This method possesses strong interpretability for subsequent electrochemical analysis inside batteries.

## 2. Methodology

### 2.1. EIS pre-process

The first part of OPDEIS is pre-processing the EIS data to obtain a suitable DRT analysis for the entire frequency range. In the timescale, interpreting the EIS curve involves analyzing different dynamic processes that contribute to the impedance response [45,46]. High-frequency responses (microseconds) involve contact polarization between particles and agglomerated fluid [47,48]. In this scenario, each battery exhibits a series inductance due to its geometric shape [49]. Furthermore, the skin effect at high frequencies constrains the depth of AC current conduction in the battery, these factors contribute to an overall increase in the ohmic resistance of the battery within high-frequency electromagnetic fields [50]. Middle-frequency responses (milliseconds) are attributed to charge transfer processes that occur at the Solid Electrolyte Interface (SEI) and Chemical Electrochemical Interface (CEI) membranes. Low-frequency responses (seconds) result from the superimposition of the diffusion process and the influence of the Open Circuit Voltage (OCV) curve [51].

In the analysis of EIS curves, Constant Phase Element (CPE) and Warburg impedance are often used to represent the response in the low-frequency range [52]. However, in the low-frequency diffusion stage of the EIS curve, the “straight line” at the end often represents the particles’ diffusion processes, which can be influenced by factors such as temperature, SOC, and other environmental or operating conditions [53]. Therefore, as shown in Equation (1), by separating the RC processes between low-frequency insertion capacitance and different time constants, we can improve the accuracy of quantitative analysis in the DRT analysis process. However, accurately calculating the size of  $C_{in}$  is a challenge. The  $C_{in}$  can be obtained by calculating the derivative of the OCV-SOC curve using Equation (2).

$$Z(f) = R_0 + R_{pol} \int_{\tau_1}^{\tau_n} \frac{g(\tau)}{1 + i2\pi f\tau} d\tau + \frac{1}{jwC_{in}} \quad (1)$$

$$C_{in} = \frac{Q_{li} dSOC}{dOCV} = \frac{dQ}{dV} \quad (2)$$

In this study, we researched three experimental methods and data processes to obtain the dOCV/dSOC and  $C_{in}$  in 25 °C. The experimental equipment used includes a charge-discharge instrument (Bipolar Power

Supply PBZ-40-10 from Japan KIKUSUI), a voltage acquisition module (Dewesoft Siriusi-HS-8xHV), and impedance spectrum test equipment (Gamry Reference 3000). Table 1 provides relevant information about the experimental battery we used. Here are the experimental procedures for the three methods:

- i) Small current pulses experiment (durations for each: 63 h)

Discharge the battery for 10% SOC each cycle from 100%SOC to 0% SOC at a discharge rate of 16 A (0.5C). After each discharge, a small current pulse is applied at a rate of 1.6 A (1/20 C) for 6 min. Following each discharge and pulse, the battery is left to rest for 3 h before the next test cycle begins.

- ii) HPPC test (durations for each: 126 h)

We obtained the SOC-OCV curve through the HPPC test (Hybrid Pulse Power Characterization). Perform an HPPC experiment at every 5% SOC with a current of 0.5C.

- iii) 1/100 C discharge experiment. (durations for each: 100 h)

A current of 0.32 A (1/100 C) is used to discharge the battery. In this case, it can be considered as applying a 2.78 μHz square wave current signal. Under this condition, the current is very small, and the fundamental and harmonic components occur in the extremely low-frequency range. The influence on voltage can be neglected. Therefore, the voltage across the battery terminals is approximately equal to the OCV [47]. Equation (3) is used to perform non-linear fitting on the obtained SOC-OCV curve with a polynomial function  $f(p,x)$ . Equation (3) adds a constraint on the derivative of the SOC-OCV curve because it accounts for the OCV decrease that occurs during discharge.  $SOC_m$  represents the obtained SOC value ranging from 0 to 1.0 in experiments (ii) and (iii), while  $SOC_n$  represents any arbitrary point within the variable range of 0–1.0 in the fitted curve.

$$\begin{cases} f(p, SOC_m) = OCV; \\ f'(p, SOC_m) = \frac{dQ}{dV}; \\ f'(p, SOC_n) \geq 0; \end{cases} \quad (3)$$

By using the gradient of the SOC-OCV curve, you can calculate the value of  $C_{in}$ , which is depicted in Fig. 1. We can see results of experiment (ii) and experiment (iii) are close in Fig. 1 (b). In terms of the trend of change, experiment (i) and experiment (iii) are similar in Fig. 1 (c). At the same time, the 1/100 C experiment contains more information and exhibits more sensitivity to curve variations, it exhibits more precise results of the overall inserted capacitance, especially at SOC = 0 or 1.0. Therefore, OPDEIS selects the curve obtained from the 1/100 C discharge as the input for  $C_{in}$ . From Fig. 1 (d), it can be observed that the introduction of  $C_{in}$  has a significant impact on the non-steady-state (SOC = 0). This enables a better analysis of the low-frequency diffusion processes.

### 2.2. DRT parameters extraction

#### 2.2.1. DRT process with inductance and $C_{in}$

After EIS Pre-PROCESS, we have achieved the fitting of low-frequency EIS. Due to electromagnetic induction phenomena and the characteristics of the measurement cables themselves, we have considered inductance and  $C_{in}$ . We use (4) to extend the DRT model to the entire frequency range.

$$Z(jw) = jwL + R_0 + R_{pol} \int_0^{\infty} \frac{g(\tau)}{1 + jw\tau} d\tau + \frac{1}{jwC_{in}} \quad (4)$$

Substituting  $t = \ln(\tau)$ , (5), (6) are obtained.

**Table 1**  
Battery specification.

Battery type	Rated capacity	resistance	Min voltage	Max voltage	Vendor
LF32 (LiFePO <sub>4</sub> )	32Ah	≤0.79 mΩ	2.5V	3.65V	EVE ENERGY CO., LTD

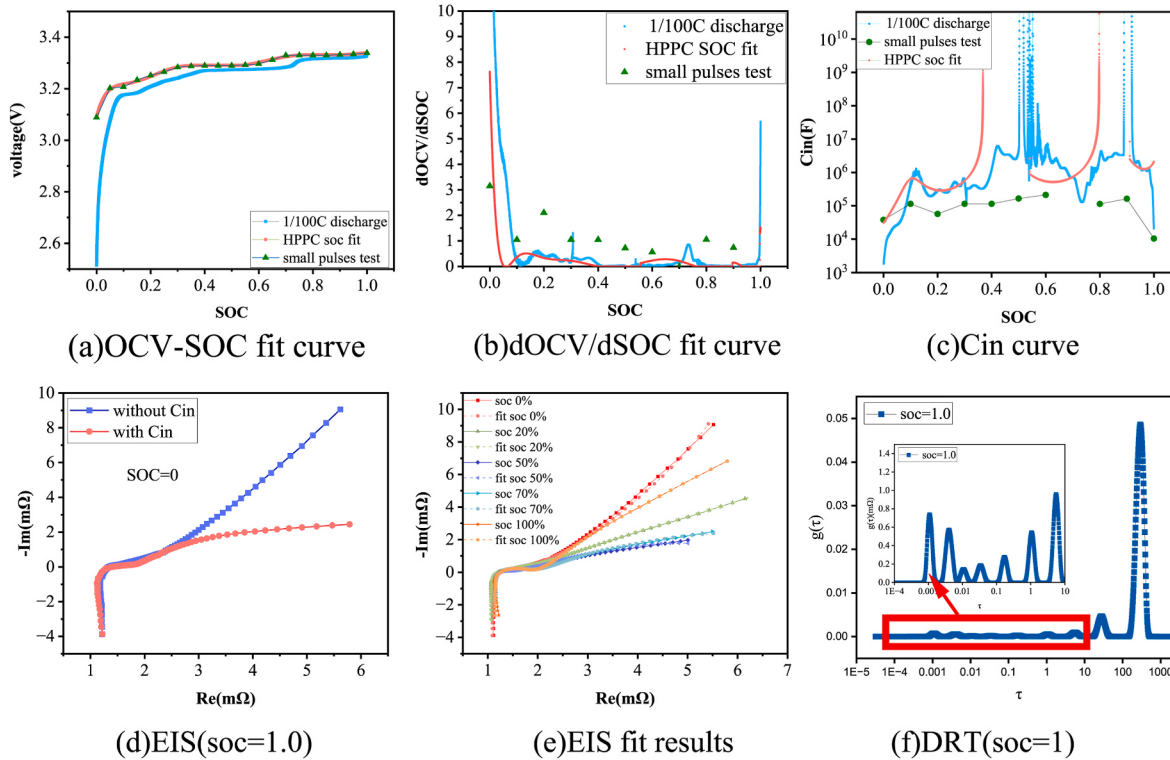


**Fig. 1.** (a) SOC-OCV curve (b) dOCV/dSOC (c)  $C_{in}$  in three methods (d) the impact of  $C$  on EIS ( $SOC = 0$ ) (e) the full-frequency range fitting results for different SOCs (f) the full-frequency range results for DRT analysis ( $SOC = 1$ ).

$$Z(jw) = jwL + R_0 + R_{pol} \int_{-\infty}^{+\infty} \frac{e^t g(e^t)}{1 + jwe^t} dt + \frac{1}{jwC_{in}} \quad (5)$$

$$Z(jw) = jwL + R_0 + \frac{1}{jwC_{in}} + R_{pol} \int_{-\infty}^{+\infty} \frac{e^t g(e^t)}{1 - (jwe^t)^2} dt - R_{pol} \int_{-\infty}^{+\infty} \frac{jwe^{2t} g(e^t)}{1 - (jwe^t)^2} dt \quad (6)$$

In this case, we typically choose a set of finite and discrete basis functions to replace  $g(e^t)$ .

$$g(e^t) = \sum_{n=1}^N X_n \varphi(t) + e_g(t) \quad (7)$$

The discrete error caused by discrete basis functions is denoted as  $e_g(t)$ , and  $e_z(x)$  is the sum of the discrete error as (8).

$$e_z(x) = \sum_{n=1}^N \left[ \frac{1}{w_n} \left( Z_{\exp}(f_n) - Z'_{fit}(X, f_n) \right)^2 + \frac{1}{w_n} \left( Z''_{\exp}(f_n) - Z''_{fit}(X, f_n) \right)^2 \right] \quad (8)$$

where  $Z'_{\exp}(f_n)$  refers to the actual impedance real part, and  $Z''_{\exp}(f_n)$  refers to the actual impedance imaginary part.  $Z'_{fit}(f_n)$  refers to the fitting impedance real part, and  $Z''_{fit}(f_n)$  refers to the fitting impedance imaginary part.

The value of  $X$  that minimizes  $e_z(x)$  is the result we prefer. Due to a large number of unknowns and measurement errors in EIS measurement, this is an ill-conditioned problem and the solution may oscillate significantly. Therefore, regularization fitting is used to address this issue.

$$e_z(x) = \|Z_{\exp}' - A'X\|_2^2 + \|Z_{\exp}'' - A''X\|_2^2 + \lambda \|LX\|_2^2 \quad (9)$$

By combining inductance and insertion capacitance, we have achieved DRT analysis across the entire frequency range. We measured the EIS using Gamry reference 3000 with 0.5 A current across the frequency range of 0.003 Hz–3000 Hz. The fitting results on the full frequency range are shown in Fig. 1 (e). The results demonstrate a strong agreement between the full frequency range fitting of EIS with this model and the actual EIS data at different SOCs. However, in the full-frequency DRT results, achieving the optimal fitting effect and capturing the dynamic processes inside the battery typically requires choosing the appropriate regularization parameter and FWHM values.

#### 2.2.2. Regularization parameter and FWHM

In this section, we studied the specific effects of regularization parameter and FWHM on the DRT fitting process. In (9), by controlling the magnitude of the regularization parameter  $\lambda$ , we can adjust the degree of penalty applied in the least squares fitting. Based on Fig. 2 (c), we can observe that as the value of  $\lambda$  increases in the RC circuit, the resulting DRT becomes smoother, but it fails to reflect the distribution characteristics of the peak. Meanwhile, when  $\lambda$  is very small, its peak becomes very steep, making it easy for false peaks or artifacts to be introduced into the fitting process.

In addition to  $\lambda$ , the FWHM of the basis functions will significantly impact the fitting results. Taking the Gaussian function in radial basis functions as an example in Fig. 2 (a), at  $t = \tau_m$ , Gaussian functions centered around  $\tau_{m-1}$  and  $\tau_{m+1}$  will both have an impact on the value at

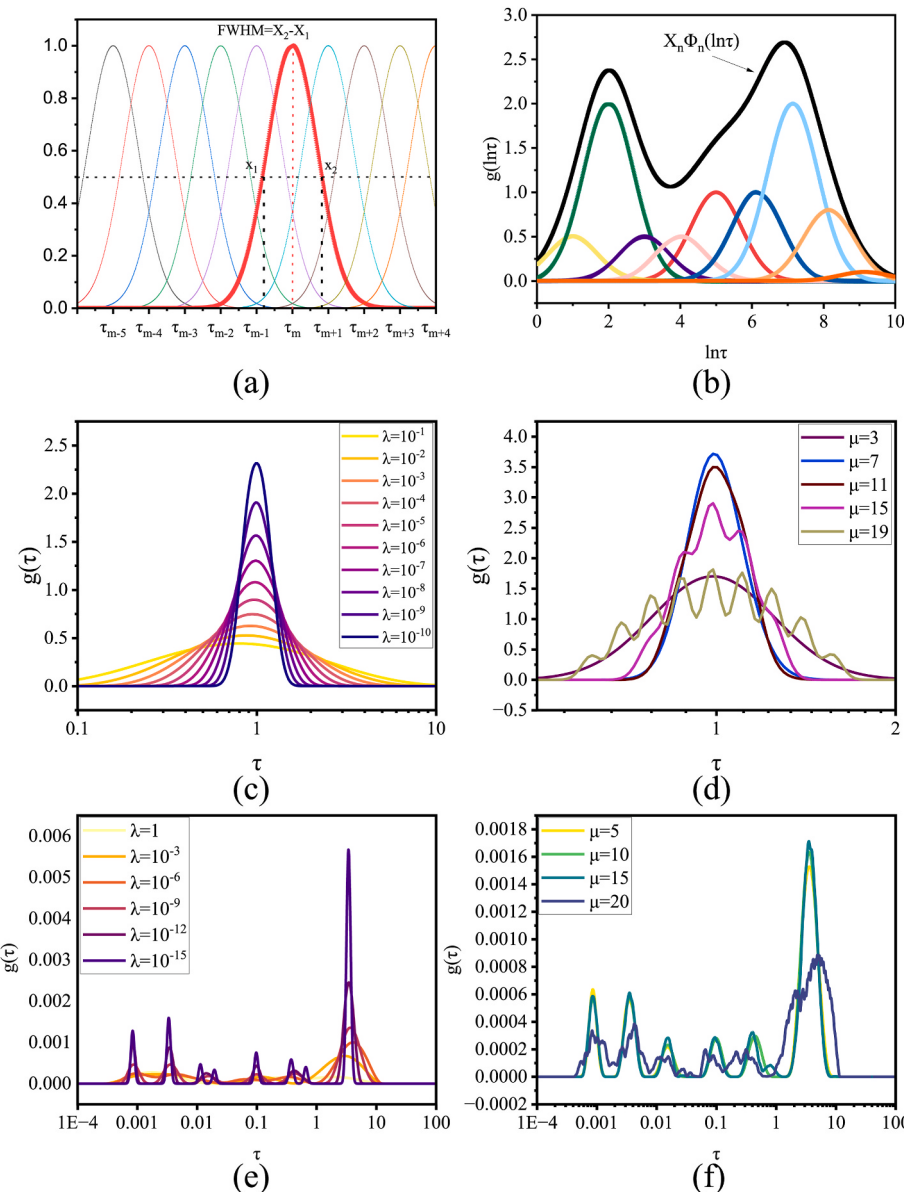


**Fig. 2.** (a) FWHM of the basic function (b) impact of basic functions on DRT results (c) DRT result of RC circuit ( $\mu = 7.159$ , FWHM =  $2\Delta\ln\tau$ ) (d) DRT result of RC circuit ( $\lambda = 10^{-12}$ ) (e) DRT result of Lithium-ion battery ( $\mu = 10.852$ , FWHM =  $2\Delta\ln\tau$ ) (f) DRT result of Lithium-ion battery ( $\lambda = 10^{-12}$ ).

$\tau_m$ . The DRT value at each point can be written as (10).

$$Z_{fit}(f_m) = \sum_{n=1}^N \left[ X_n \int_{-\infty}^{+\infty} \varphi_n(\tau) \left( \frac{1}{1 + (2\pi f_m \tau)^2} \right) d\ln\tau \right] - i \times \sum_{n=1}^N \left[ X_n \int_{-\infty}^{+\infty} \varphi_n(\tau) \left( \frac{2\pi f_m \tau}{1 + (2\pi f_m \tau)^2} \right) d\ln\tau \right] + e_z(f) \quad (10)$$

When calculating the impedance value, all basis functions corresponding to time constants are calculated by (10). From Fig. 2 (b), it is evident that the final function  $g(\ln\tau)$  is a combination of basis functions with varying sizes. At each point, the distributions of the different basis functions interact with each other. The FWHM parameter, representing the width of each basis function, determines the level of coupling between them in the  $\ln\tau$  domain. The parameter  $\mu$  can indeed be used to represent the size of FWHM in (11) as the basis function are Gaussian function.

$$f(x) = e^{-(\mu x)^2} \quad (11)$$

$$\mu = \frac{2\sqrt{\ln 2}}{FWHM}$$

In Fig. 2 (d), when  $\mu = 3$ , the resulting curve appears too flat and cannot accurately capture the desired relaxation distribution characteristics. On the other hand, selecting a narrower width ( $\mu = 19$ ), the oscillation phenomenon becomes more prominent. Fig. 2 (e) and (f) show the impact of two parameters on the impedance of lithium-ion batteries (0.1 Hz–3000 Hz, ppd = 30). We can observe that under the influence of multiple peaks in lithium-ion batteries, large values of  $\mu$  and small values of  $\lambda$  lead to more pronounced oscillations and false peaks. On the other hand, small values of  $\mu$  and large values of  $\lambda$  can indeed result in a lack of discrimination between different peaks. Therefore, we need a new method to carefully select appropriate values of  $\mu$  and  $\lambda$  that balance capturing the peaks' characteristics and avoiding artifacts or lack of discrimination.

### 2.3. Automated optimization

#### 2.3.1. Optimization objectives

OPDEIS utilizes an improved multi-objective particle swarm optimization algorithm (MOPSO-DRT) to dynamically select the  $\lambda$  and  $\mu$ . This paper transforms the parameter selection into an optimization problem and proposes two metrics for describing overfitting and underfitting issues.

##### i) Error Index

In order to describe the accuracy of the selection, we use (12) to evaluate the result. The smaller the  $R_{opt}^2$ , the higher the accuracy of the fitting. It can solve the problem of increased errors caused by a curve being too smooth or oscillating.

$$R_{opt}^2 = \frac{1}{N} \sum_{n=1}^N \left[ \left( \frac{Z'_{exp}(f_n) - Z'_{fit}(f_n)}{Z'_{exp}(f_n)} \right)^2 + \left( \frac{Z''_{exp}(f_n) - Z''_{fit}(f_n)}{Z''_{exp}(f_n)} \right)^2 \right] \quad (12)$$

##### ii) Smoothness Index

OPDEIS proposes the smoothness index as another optimization criterion to achieve a smoother DRT result. In previous studies, it has been observed that the parameter  $\mu$  has an impact on the steepness and oscillation of peaks. For characterizing the behavior of multiple unknown peaks in the DRT process, selecting the variance of curvature as a measure of the steepness of the peaks can be a suitable approach. We calculate the curvature of the distribution function at each point using (13). At the same time, artifacts and oscillation of the peaks can be represented by the number of extremal points. Then the smoothness index of the DRT result can be determined by (14).

$$K_i = \left| \frac{\arctan\left(\frac{g(\tau_{i+2})-g(\tau_{i+1})}{\tau_{i+2}-\tau_{i+1}}\right) - \arctan\left(\frac{g(\tau_{i+1})-g(\tau_i)}{\tau_{i+1}-\tau_i}\right)}{\sqrt{(\tau_{i+1}-\tau_i)^2 + (g(\tau_{i+1})-g(\tau_i))^2}} \right| \quad (13)$$

$$Idx_{smth} = Sch * 100 * Var(K(\tau)) \quad (14)$$

where  $Sch$  is the number of points where the derivative of the function  $g$  is equal to 0.

In our result, since the variance of  $K$  is typically between  $10^{-4}$  and  $10^{-6}$ . To expand the value range of the  $Idx_{smth}$  for better optimization and extraction, we multiply it by 100 to ensure a larger difference and facilitate optimization. In this way,  $Idx_{smth}$  solves the problem of spurious peaks and oscillation in overfitting.

Thus, we can obtain the final objective function.

$$\begin{aligned} & \min_x E_{index}(\lambda, \mu, f(x)) \\ & \min_x \text{smoothness\_index}(\lambda, \mu, f(x)) \end{aligned} \quad (15)$$

where  $f(x)$  is the final obtained distribution function result. By incorporating these two objectives, we aim to achieve a smooth and accurate result that effectively captures the essential characteristics of the peaks while minimizing any artifacts or lack of discrimination.

#### 2.3.2. MOPSO-DRT

This paper employs a specific Multi-Objective (MOPSO) algorithm tailored to address the problem. The algorithm utilizes the Pareto frontier to handle the parameter selection problem. Furthermore, the paper proposes a distributed grid partitioning method to extract the optimal solutions from the Pareto frontier. The specific process is illustrated in Fig. 3.

The preprocessed data is input into OPDEIS. In this study, 100 particles are chosen for the search. The regularization parameter is selected using a logarithmic scale. This means that the search range for  $\lambda$  is

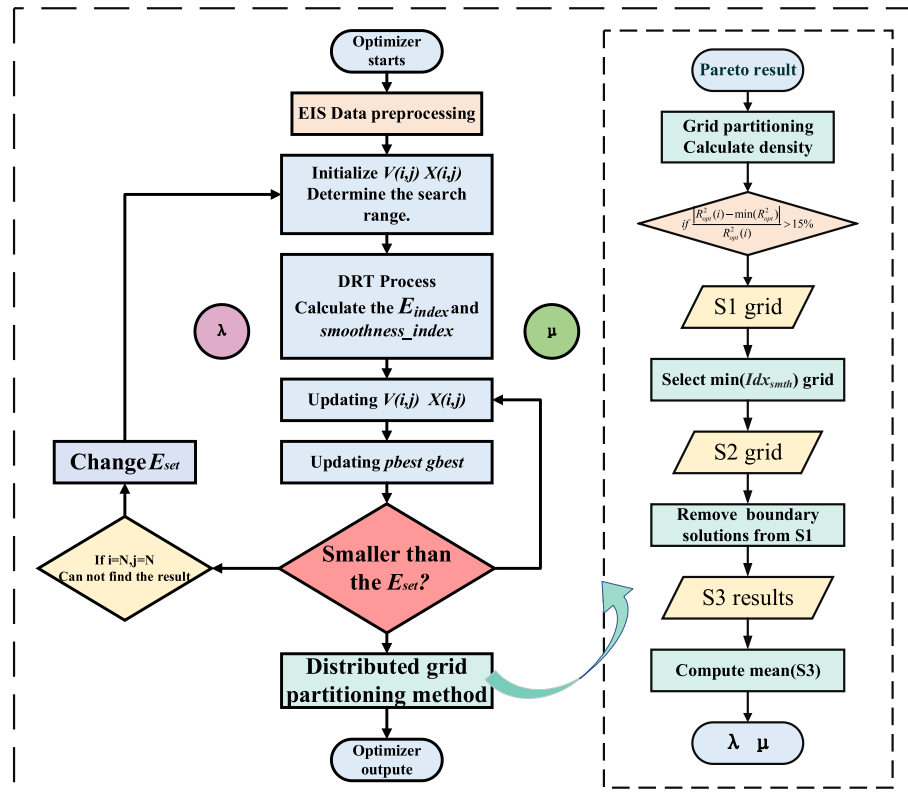


Fig. 3. The workflow of MOPSO-DRT.

defined from 0 to 15, and the regularization parameter is defined as  $10^{-\lambda}$ . Set the search range for the  $\mu$  so that FWHM ranges from  $\Delta \ln \tau / 10$  to  $10 \Delta \ln \tau$ . In each iteration, DRT analysis was calculated and we can obtain  $R_{\text{opt}}^2$  and  $Idx_{\text{smth}}$  as the fitness function values of the particles.

OPDEIS introduces an accelerated automatic optimization framework in MOPSO. If the solution's  $R_{\text{opt}}^2$  is greater than the predefined threshold value  $E_{\text{set}}$ , it is defined as a dominated solution to be discarded. In the context of DRT fitting results, accuracy is more important.  $E_{\text{set}}$  can be set by the user, and typically it is set to 0.1. This constraint is applied to accelerate the convergence speed to within 25 iterations. If the optimal solution is not found after all iterations (50 iterations), the value of  $E_{\text{set}}$  can be automatically added to find the optimal result at a lower accuracy.

We investigated the parameter distribution patterns of lithium batteries and proposed a distributed grid partitioning method. Fig. 4 shows the  $R_{\text{opt}}^2$  and  $Idx_{\text{smth}}$  of the lithium battery's EIS data under different parameters.

Based on Fig. 4, it is evident that using excessively large or small values of  $\lambda$  or  $\mu$  will lead to an increase in the  $R_{\text{opt}}^2$ . Furthermore, as  $\mu$  decreases and  $\lambda$  increases, the  $Idx_{\text{smth}}$  tends to decrease as well. Consequently, when searching for the optimal value from the Pareto solution set, it is advisable to exclude the maximum and minimum parameter marginal values.

Obtaining the optimal solution from the Pareto set is indeed a challenge, and the distributed grid partitioning method proposed in this paper provides an effective solution. OPDEIS uses grids to partition the solutions, with grid size ( $\lambda = 1$ ,  $\mu = 2$ ). Fig. 5 illustrates the specific extraction process.

- First, it obtains a series of solution sets **S1** with the lowest  $R_{\text{opt}}^2$  values within a 15% margin of error.
- Second, find the minimum smoothness index value  $Smooth_{\text{min}}$  from **S1**. Then it gets the solutions **S2** where  $Idx_{\text{smth}}$  less than  $5Smooth_{\text{min}}$  from **S1**.
- Finally, obtain **S3** by computing the grid coordinates for each solution in **S2** and removing sparse solutions that are far away from the majority of solutions. We take the average value of  $\lambda$  and  $\mu$  in **S3** as the optimal output solution for OPDEIS.

### 3. Result and discussion

#### 3.1. Validation

By systematically verifying the accuracy, stability, practicality, and reliability of the method through simulation, experimentation, and the analysis of lithium-ion battery data, we can establish its credibility and potential in battery-related applications. The algorithm described in this paper was implemented and the results were computed using MATLAB. We validated with single and multiple parallel RC models, as well as lithium battery EIS. The optimal Pareto sets were obtained after 13, 19,

and 22 iterations respectively. The entire optimization results of the OPDEIS are shown in Fig. 5.

#### 3.1.1. RC model

To demonstrate the accuracy of this method for obtaining results, we conducted a test using a first-order RC model. In the first-order RC model used in this study,  $R = 5 \Omega$ ,  $C = 1 \text{ F}$ ,  $\tau = 1 \text{ s}$ , frequency = 0.1 Hz–1000 Hz, ppd = 250. Fig. 5 (a) series illustrates the process of obtaining the optimal solution from the Pareto front in the OPDEIS for the RC model. It is visually apparent that the optimal solution should lie within the three grids between (12, 6) and (14, 10) shown in Fig. 5 (a-3). The optimal solution obtained by OPDEIS calculation is  $\lambda = 10^{-13.436173}$ ,  $\mu = 8.6540435$ , FWHM =  $2.417668 \Delta \ln \tau$ ,  $R_{\text{opt}}^2 = 2.4734 \text{ e}^{-4}$ ,  $Idx_{\text{smth}} = 0.3397$ . Fig. 6 (a) and (b) show the fitting and DRT results of EIS, from which we can see that the fitting result highly overlaps with the exact EIS, along with the absence of pseudo peaks. Moreover, in the DRT results, the distribution of the time constant is in accordance with the preset value of 1 s, and the peak amplitude is also close to the preset value of 5  $\Omega$ . This indicates that the optimal result accurately captures the distribution of relaxation times within the RC.

#### 3.1.2. 2-Orders RC models

To further investigate the accuracy and reliability of this method under the coupling effect of multiple RC processes, we conducted tests using a second-order RC model as shown in (16).

$$Z(f) = R_{\infty} + \frac{R_1}{1 + (i2\pi f\tau_1)} + \frac{R_2}{1 + (i2\pi f\tau_2)} \quad (16)$$

In the model,  $R_{\infty} = 10 \Omega$ ,  $R_1 = 10 \Omega$ ,  $R_2 = 5 \Omega$ ,  $\tau_1 = 0.01 \text{ s}$ ,  $\tau_2 = 1 \text{ s}$ . The grid within the red box in Fig. 5 (b-3) visually depicts the distribution of the optimal solution. The optimal solution obtained by OPDEIS is  $\lambda = 10^{-13.084267}$ ,  $\mu = 7.43859$ , FWHM =  $2.07811 \Delta \ln \tau$ ,  $R_{\text{opt}}^2 = 5.2595 \text{ e}^{-5}$ ,  $Idx_{\text{smth}} = 0.0973$ . In Fig. 6 (c) and (d), the peak value corresponds to time constants of 1 s and 0.01 s, and the first peak value is 32.1018, the second peak value is 16.0325, and their ratio is 2.0023, which accurately reflects the relationship between  $R_1$  and  $R_2$  in terms of their relative sizes. At this point, the optimization results can effectively decouple the two RC processes and accurately reflect the role of the time constant.

#### 3.1.3. Lithium-ion batteries

After ensuring the reliability and robustness of OPDEIS, we will apply it to the DRT analysis of lithium batteries. Fig. 1 (f) presents the full-frequency DRT analysis results, revealing that due to the low-frequency diffusion phenomenon, the optimized DRT results are mainly dominated by the EIS below 0.1 Hz. However, the polarization process in the high-frequency range is more significant in the battery. Therefore, further optimization and discussion are carried out using OPDEIS for EIS above 0.1 Hz in lithium batteries. We conduct EIS testing on the battery (3000 Hz–0.1 Hz, ppd = 30, SOC = 1.0) used in section 2

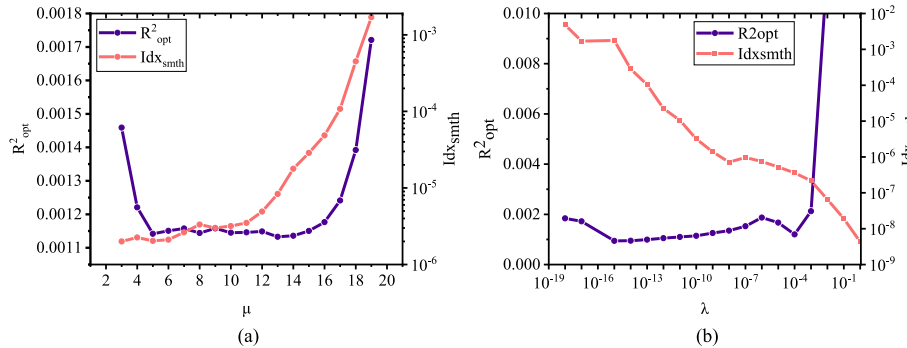


**Fig. 4.** The change of  $R_{\text{opt}}^2$  and  $Idx_{\text{smth}}$ . (a)  $\lambda = 10^{-10}$  (b)  $\mu = 10.852$ , FWHM =  $2 \Delta \ln \tau$ .

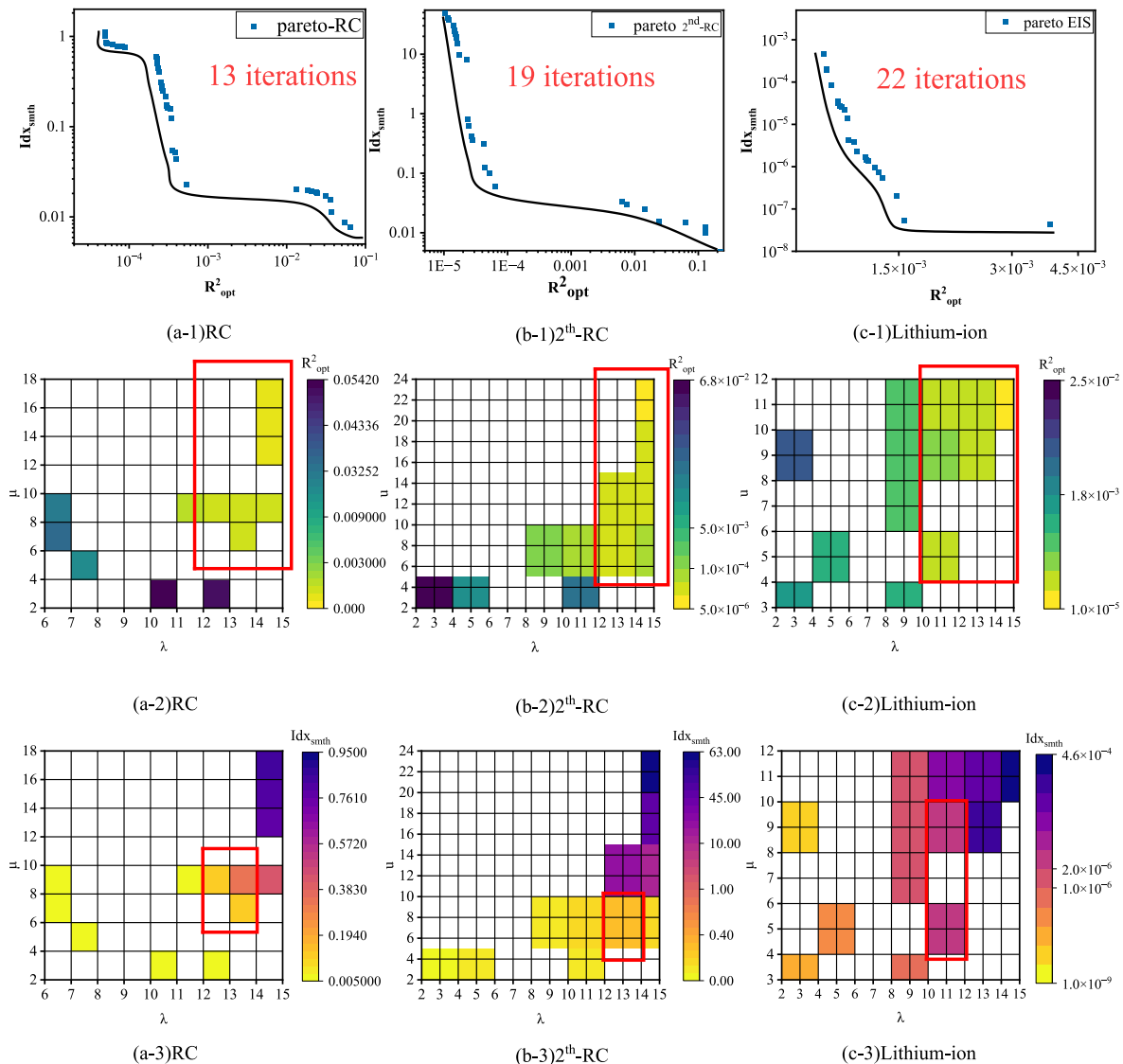


**Fig. 5.** Distributed grid partitioning method (a-1) (b-1) (c-1) represents the Pareto optimal solution set after OPDEIS iterations. (a-2) (b-2) (c-2) are the steps for extracting “S1” based on  $R_{opt}^2$  for RC, 2-orders RC models, and lithium-ion batteries; (a-3) (b-3) (c-3) are the steps for extracting “S2” based on  $Idx_{smth}$  for RC, 2-orders RC models and lithium-ion batteries.

using the Gamry Reference 3000.

In Fig. 6 (e), it is observed that the measured EIS data has errors at certain points. This helps determine how well OPDEIS mitigates the impact of data errors and improves the accuracy and reliability of the analysis. Fig. 5 (c-3) illustrates the position of the optimal solution, and after excluding sparse solutions, we obtain the optimal solution for the lithium battery data:  $\lambda = 10^{-10.8611}$ ,  $\mu = 9.53926$ , FWHM =  $1.75806\Delta\ln\tau$ ,  $R_{opt}^2 = 0.0115$ ,  $Idx_{smth} = 2.1164e^{-5}$ . In Fig. 6 (e), the fitted EIS data is smoother and highly consistent with the measured data, six distinct peaks are observed, and no false peaks appear in Fig. 6 (f). After removing the inductive effect, the time constant of P1 is less than  $10^{-3}$ , and from Fig. 7 (b), it can be observed that P1 is almost independent of SOC variation. Therefore, P1 represents the process of contact polarization between the active material and the current collector [48]. The peak of P2 is similar to that of P1, with a time constant of less than  $10^{-2}$ . The occurrence time of P3 is close to P2, and the peak of P3 is very small. Therefore, P2 and P3 are likely manifestations of the SEI membrane polarization process [46]. P4 and P5 have time constants less than 1 s, indicating multiple processes, and they may be manifestations of the charge transfer reaction polarization process and double-layer capacitance effect [47]. The peak P6 is very large and occurs at a time

greater than 1 s, indicating a low-frequency diffusion process.

The purpose of OPDEIS is to enable users to obtain the optimal regularization parameters and FWHM for different frequency ranges based on different EIS frequency points when analyzing the DRT of lithium batteries. To ensure its universality and applicability, we conducted tests using data at various ppd. Table 2 presents the optimized parameters obtained and Fig. 7 (a) displays the DRT results corresponding to the optimized parameters. The fitting errors of the optimized results are all within 1.15%. When the ppd is larger than 5, the DRT analysis successfully separates distinct peaks without the presence of any spurious peaks. However, when ppd = 5, and only 14 useable fitting points are available after removing the high-frequency range, it inevitably results in increased fitting errors and makes it more challenging to differentiate between different polarization processes. Despite these challenges, OPDEIS still manages to identify the optimal parameters that reflect the corresponding time constants in different frequency ranges as shown in Fig. 7 (a). This showcases the robustness and effectiveness of OPDEIS in capturing the underlying polarization processes.

Finally, we further validated the reliability of the parameters obtained through OPDEIS by conducting experiments on lithium batteries

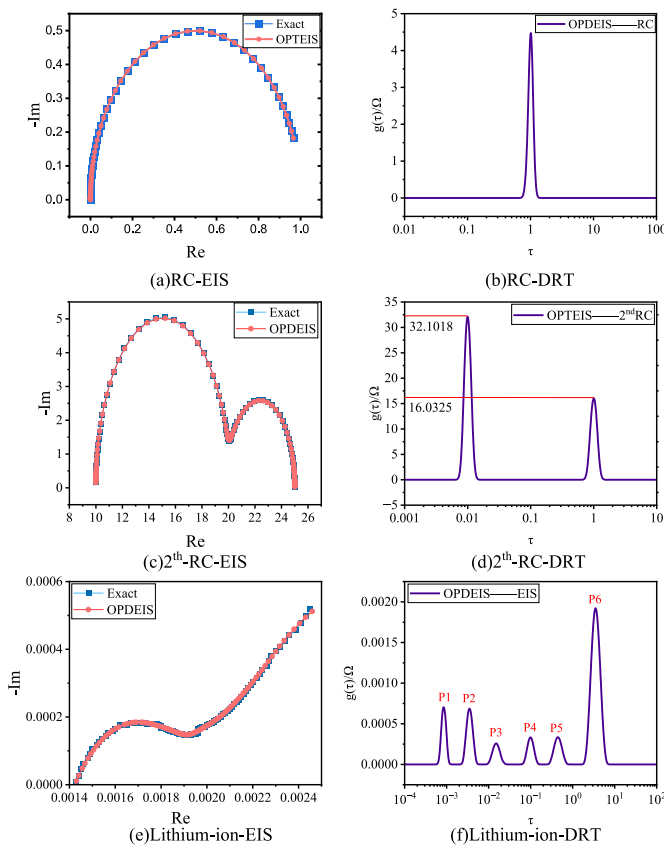


**Fig. 6.** Optimized DRT results. (a) (c) (e) are EIS fitting results for RC, 2-orders RC models, and lithium-ion batteries; (b) (d) (f) are the DRT results for RC, 2-orders RC models, and lithium-ion batteries.

at different SOC levels. From Fig. 7 (b), it can be observed that as SOC changes from 0 to 1.0, there is a significant variation in the peak values in the low-frequency range, and there is also a subtle variation in the ratio between the two peaks in the high-frequency range. This also highlights that OPDEIS can effectively and accurately provide pre-processing for DRT analysis.

Indeed, there is still ongoing research on how to obtain more comprehensive and accurate DRT analysis using fewer frequency points. Moreover, establishing a specific relationship between DRT and SOC, SOH, etc., based on the OPDEIS results for determining the frequency points, still poses a significant challenge.

#### 4. Conclusions

OPDEIS proposed in this paper is an effective pre-calculation DRT tool of EIS. It first eliminates the influence of the low-frequency insert capacitance on the subsequent results. This article proves that the small current discharge method with 1/100 C is more suitable for calculating the insert capacitance. Through this method, this paper extends the DRT analysis to 1 mHz for LiFePO<sub>4</sub> batteries and focuses on the analysis of EIS data above 0.1Hz.

OPDEIS aims to obtain accurate and well-regularized parameters through two objectives: error index ( $R_{\text{opt}}^2$ ) and smoothness index ( $\text{Idx}_{\text{smth}}$ ). Additionally, it takes into account the FWHM parameter, which is often overlooked but important. Compared to traditional optimization methods, OPDEIS utilizes a multi-objective particle swarm optimization method and offers an automatic constrained search mode without computing all possible regularization parameters and basis function widths. This mode significantly reduces the number of computations required and ultimately achieves parameter selection for lithium-ion battery EIS in less than 25 iterations. In terms of data

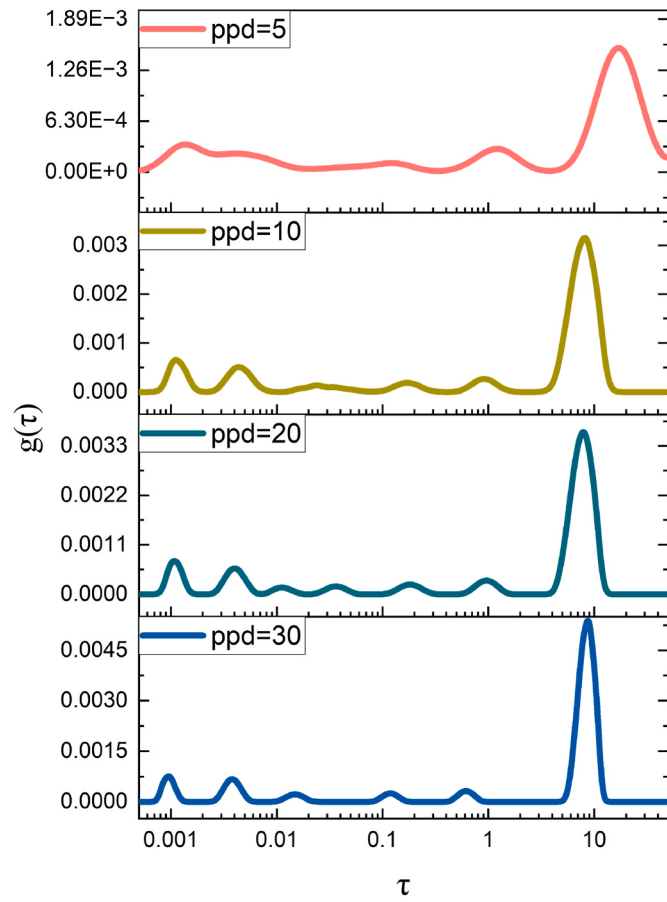


**Fig. 7.** (a) The optimal results of DRT of different ppds. (b) The optimal results of DRT of SOCs (ppd = 30, 3000 Hz–0.1 Hz).

processing, OPDEIS integrates the characteristics of lithium-ion battery EIS and introduces a distributed grid partitioning method to extract the optimal solution from the Pareto set of multiple objectives.

The validation was conducted using the RC models and lithium-ion

**Table 2**

The optimization results of lithium battery parameters with different ppd.

	$R_{\text{opt}}^2$	$\text{Idx}_{\text{smt}}$	$\lambda$	$\mu$	FWHM
ppd = 30	0.0115	$2.1164 \times 10^{-5}$	$10^{-10.8611}$	9.53926	$1.75806 \Delta \ln \tau$
ppd = 20	0.0021	$2.80128 \times 10^{-4}$	$10^{-10.38825}$	7.514933	$2.0856 \Delta \ln \tau$
ppd = 10	0.0033	$4.8824 \times 10^{-4}$	$10^{-9.742448}$	5.185193	$2.8659 \Delta \ln \tau$
ppd = 5	0.0092	$9.83369 \times 10^{-12}$	$10^{-6.38971}$	1.77413	$1.962 \Delta \ln \tau$

battery data at different frequency points. The accuracy of lithium batteries was found to be 1.15% (ppd = 30), 0.21% (ppd = 20), 0.33% (ppd = 10), and 0.92% (ppd = 5). OPDEIS is capable of being applied to EIS at different SOC and ppd conditions. Its automatic optimization approach effectively addresses the underfitting and overfitting issues that may arise during the DRT process.

### CRediT authorship contribution statement

**Pengcheng Niu:** Project administration, Methodology, Investigation, Funding acquisition, Formal analysis, Data curation, Conceptualization, Resources, Software, Supervision, Validation, Visualization, Writing – original draft, Writing – review & editing. **Kun Yang:** Conceptualization, Data curation, Methodology. **Zhengxiang Song:** Conceptualization, Funding acquisition. **Zheyuan Pang:** Software, Validation. **Zhuoyu Feng:** Validation. **Jinhao Meng:** Writing – review & editing, Conceptualization.

### Declaration of competing interest

The authors declare that they have no known competing financial interests or personal relationships that could have appeared to influence the work reported in this paper.

### Data availability

Data will be made available on request.

### Acknowledgements

This work has been funded by the National Key R&D Program of China under Grant (2023YFB2408201).

### References

- [1] M. Waseem, et al., Battery technologies and functionality of battery management system for EVs: current status, key challenges, and future perspectives, *J. Power Sources* 580 (2023).
- [2] W. Li, et al., Electrochemical failure results inevitable capacity degradation in Li-ion batteries—a review, *Energies* 15 (23) (2022).
- [3] B. Akkinappally, et al., Temperature effect and kinetics,  $\text{Li}_2\text{Zr}_2(\text{PO}_4)_3$  and  $\text{Li}_{1.2}\text{Al}_{0.2}\text{Zr}_{1.8}(\text{PO}_4)_3$  and electrochemical properties for rechargeable ion batteries, *Int. J. Energy Res.* 46 (10) (2022) 14116–14132.
- [4] A. Densmore, M. Hanif, Determining battery SOC using electrochemical impedance spectroscopy and the extreme learning machine, in: 2015 IEEE 2nd International Future Energy Electronics Conference (IFEEC), 2015. IEEE.
- [5] H. Blanke, et al., Impedance measurements on lead–acid batteries for state-of-charge, state-of-health and cranking capability prognosis in electric and hybrid electric vehicles, *J. Power Sources* 144 (2) (2005) 418–425.
- [6] A. Zenati, et al., Estimation of the SOC and the SOH of li-ion batteries, by combining impedance measurements with the fuzzy logic inference, in: IECON 2010-36th Annual Conference on IEEE Industrial Electronics Society, 2010. IEEE.
- [7] J. Xu, et al., A new method to estimate the state of charge of lithium-ion batteries based on the battery impedance model, *J. Power Sources* 233 (2013) 277–284.
- [8] D. Andre, et al., Characterization of high-power lithium-ion batteries by electrochemical impedance spectroscopy. II: modelling, *J. Power Sources* 196 (12) (2011) 5349–5356.
- [9] S. Buteau, J. Dahn, Analysis of thousands of electrochemical impedance spectra of lithium-ion cells through a machine learning inverse model, *J. Electrochem. Soc.* 166 (8) (2019) A1611–A1622.
- [10] W. Choi, et al., Modeling and applications of electrochemical impedance spectroscopy (EIS) for lithium-ion batteries, *Journal of Electrochemical Science and Technology* 11 (1) (2020) 1–13.
- [11] J. Li, et al., Remaining useful life prediction of lithium-ion batteries via an EIS-based deep learning approach, *Energy Rep.* 10 (2023) 3629–3638.
- [12] V. Bongiorno, et al., Exploring the use of machine learning for interpreting electrochemical impedance spectroscopy data: evaluation of the training dataset size, *Corrosion Sci.* 198 (2022) 110119.
- [13] B.-R. Chen, et al., A mathematical approach to survey electrochemical impedance spectroscopy for aging in lithium-ion batteries, *Front. Energy Res.* 11 (2023) 167.
- [14] Y.-H. Lin, et al., Physics-informed deep learning for lithium-ion battery diagnostics using electrochemical impedance spectroscopy, *Renew. Sustain. Energy Rev.* 188 (2023) 113807.
- [15] S. Zhu, et al., Equivalent circuit model recognition of electrochemical impedance spectroscopy via machine learning, *J. Electroanal. Chem.* 855 (2019) 113627.
- [16] Y. Lu, et al., The timescale identification decoupling complicated kinetic processes in lithium batteries, *Joule* 6 (6) (2022) 1172–1198.
- [17] D.A. Osinkin, Detailed analysis of electrochemical behavior of high-performance solid oxide fuel cell using DRT technique, *J. Power Sources* 527 (2022).
- [18] D.A. Osinkin, Complementary effect of ceria on the hydrogen oxidation kinetics on Ni - Ce<sub>0.85</sub>Mn<sub>0.20</sub>-δ anode, *Electrochim. Acta* 330 (2020).
- [19] D.A. Osinkin, Identification of gas diffusion phenomena on highly active Ni-ceramic anodes using the DRT technique, *J. Power Sources* 571 (2023).
- [20] E.A. Il'ina, D.A. Osinkin, Interpretation of the resistance of  $\text{Li}_7\text{La}_3\text{Zr}_2\text{O}_{12} - \text{Li}_{20-\delta}\text{B}_{20-\delta}\text{Si}_{\delta}\text{O}_{2\delta}$  composite electrolytes for all-solid-state batteries using the distribution of relaxation times technique, *J. Power Sources* 580 (2023).
- [21] B. Yang, et al., Electrochemical impedance preprocessing with the distribution of relaxation time transform, *J. Power Sources* 571 (2023) 233062.
- [22] H. Chen, et al., Structure-conduction correlations in a chlorine-rich superionic lithium-argyrodite solid electrolyte: a DRT analysis, *J. Power Sources* 583 (2023) 233579.
- [23] J. Wang, et al., High-efficient prediction of state of health for lithium-ion battery based on AC impedance feature tuned with Gaussian process regression, *J. Power Sources* 561 (2023) 232737.
- [24] M. Saccoccio, et al., Optimal regularization in distribution of relaxation times applied to electrochemical impedance spectroscopy: ridge and Lasso regression methods - a theoretical and experimental study, *Electrochim. Acta* 147 (2014) 470–482.
- [25] T.H. Wan, et al., Influence of the discretization methods on the distribution of relaxation times deconvolution: implementing radial basis functions with DRTtools, *Electrochim. Acta* 184 (2015) 483–499.
- [26] A.B. Tesler, et al., Analyzing results of impedance spectroscopy using novel evolutionary programming techniques, *J. Electroceram.* 24 (4) (2009) 245–260.
- [27] B. Py, et al., Gaussian processes for the analysis of electrochemical impedance spectroscopy data: prediction, filtering, and active learning, *Electrochim. Acta* 439 (2023).
- [28] A. Maradesa, et al., The probabilistic deconvolution of the distribution of relaxation times with finite Gaussian processes, *Electrochim. Acta* 413 (2022).
- [29] T. Hörlin, Deconvolution and maximum entropy in impedance spectroscopy of noninductive systems, *Solid State Ionics* 107 (3–4) (1998) 241–253.
- [30] J.P. Schmidt, et al., The distribution of relaxation times as basis for generalized time-domain models for Li-ion batteries, *J. Power Sources* 221 (2013) 70–77.
- [31] X. Zhou, et al., Impedance characterization of lithium-ion batteries aging under high-temperature cycling: importance of electrolyte-phase diffusion, *J. Power Sources* 426 (2019) 216–222.
- [32] P. Iurilli, et al., EIS2MOD: a DRT-based modeling framework for Li-ion cells, *IEEE Trans. Ind. Appl.* 58 (2) (2022) 1429–1439.
- [33] P. Iurilli, et al., On the use of electrochemical impedance spectroscopy to characterize and model the aging phenomena of lithium-ion batteries: a critical review, *J. Power Sources* 505 (2021).
- [34] T.H. Wan, et al., Influence of the discretization methods on the distribution of relaxation times deconvolution: implementing radial basis functions with DRTtools, *Electrochim. Acta* 184 (2015) 483–499.
- [35] M. Saccoccio, et al., Optimal regularization in distribution of relaxation times applied to electrochemical impedance spectroscopy: ridge and Lasso regression methods - a theoretical and experimental study, *Electrochim. Acta* 147 (2014) 470–482.
- [36] Jakob Hansen, et al., Non-negatively Constrained Least Squares and Parameter Choice by the Residual Periodogram for the Inversion of Dielectric Relaxation Spectra: Supplementary Materials" Math. NA, 2014.
- [37] J.K. Hansen, J.D. Hogue, G.K. Sander, R.A. Renaut, S.C. Popat, Non-negatively constrained least squares and parameter choice by the residual periodogram for the inversion of electrochemical impedance spectroscopy data, *J. Comput. Appl. Math.* 278 (2015) 52–74. Apr.
- [38] X. Li, et al., Deconvolving distribution of relaxation times, resistances and inductance from electrochemical impedance spectroscopy via statistical model selection: exploiting structural-sparsity regularization and data-driven parameter tuning, *Electrochim. Acta* 313 (2019) 570–583.
- [39] N. Schlüter, et al., Direct access to the optimal regularization parameter in distribution of relaxation times analysis, *Chemelectrochem* 7 (16) (2020) 3445–3458.
- [40] N. Schlüter, et al., Finding the optimal regularization parameter in distribution of relaxation times analysis, *Chemelectrochem* 6 (24) (2019) 6027–6037.
- [41] M. Hahn, et al., Optimized process parameters for a reproducible distribution of relaxation times analysis of electrochemical systems, *Batteries* 5 (2) (2019).

- [42] Y. Zhang, et al., A high-precision approach to reconstruct distribution of relaxation times from electrochemical impedance spectroscopy, *J. Power Sources* 308 (2016) 1–6.
- [43] A.L. Gavrilyuk, et al., On a variation of the Tikhonov regularization method for calculating the distribution function of relaxation times in impedance spectroscopy, *Electrochim. Acta* 354 (2020).
- [44] D. Zhu, et al., Optimization and application of the distribution of relaxation times based on characteristic frequency resolution and hyperparameters, *J. Power Sources* 545 (2022).
- [45] R.K. Tagayi, et al., Employment of relaxation times distribution with improved elastic net regularization for advanced impedance data analysis of a lithium-ion battery, *J. Energy Storage* 70 (2023).
- [46] C. Brivio, et al., A physically-based electrical model for lithium-ion cells, *IEEE Trans. Energy Convers.* 34 (2) (2019) 594–603.
- [47] M. Derakhshan, et al., Detecting mechanical indentation from the time constants of Li-ion batteries, *Cell Reports Physical Science* 3 (11) (2022).
- [48] X. Zhou, et al., Impedance characterization of lithium-ion batteries aging under high-temperature cycling: importance of electrolyte-phase diffusion, *J. Power Sources* 426 (2019) 216–222.
- [49] A. Jossen, Fundamentals of battery dynamics, *J. Power Sources* 154 (2) (2006) 530–538.
- [50] N. Kularatna, Dynamics and Modeling of Rechargeable Batteries: what electrochemists? work tells the electronic engineers, *IEEE Power Electronics Magazine* 1 (4) (2014) 23–33.
- [51] N. Kularatna, Dynamics and Modeling of Rechargeable Batteries: what electrochemists? work tells the electronic engineers, *IEEE Power Electronics Magazine* 1 (4) (2014) 23–33.
- [52] Q. Zhang, et al., Degradation mechanism analysis and State-of-Health estimation for lithium-ion batteries based on distribution of relaxation times, *J. Energy Storage* 55 (2022).
- [53] X. Zhao, et al., On full-life-cycle SOC estimation for lithium batteries by a variable structure based fractional-order extended state observer, *Appl. Energy* 351 (2023).